Convection-Induced Absorption Oscillations in a Cuvette after Irradiation of a Pentazadiene Solution by Laser Pulses

Fritz Gassmann,* Thomas Lippert, Jiang Wei, and Alexander Wokaun

Paul Scherrer Institute, CH-5232 Villigen-PSI, Switzerland

Received: September 6, 2001; In Final Form: January 17, 2002

After irradiation of a pentazadiene solution (in THF) in a cuvette by laser pulses, damped oscillations of the absorbance were observed and mistakenly interpreted as being of photochemical origin. Additional experiments gave results that were incompatible with our photochemical interpretation and led to the identification of convection as the physical mechanism behind the observed oscillations. A simulation model based on the Navier−Stokes equations reproduces the damped oscillations. Analytical formulas are given to estimate convection velocities in cuvettes and might help to prevent misinterpretation of photolysis experiments. They show that arbitrarily small horizontal temperature gradients lead to convection in even very thin cuvettes. In any standard temperature-controlled cuvette, the fluid has to be assumed to be in motion rather than at rest.

Introduction

The first homogeneous chemical oscillator was observed in 1921 by W. C. Bray, and 30 years later, B. P. Belousov discovered another type of a homogeneous chemical oscillator (published only in 1958 because scientific journals rejected its publication for 7 years). Supported by models of A. M. Zhabotinskii and I. Prigogine in the 1960s and of R. J. Field, E. Körös and R. M. Noyes in the early 1970s, the reality of chemical oscillations in homogeneous solutions is now generally accepted.[1] Due to biological implications, the interest for new and different chemical oscillators is still very high. On this background, observations of unusual absorbance oscillations occurring after irradiation of a pentazadiene solution by laser pulses triggered our interest and our attempts to interpret them on a photochemical basis.[2] However, as we will show in this paper, the observed damped oscillations were caused by convection and not by photochemical reactions. We would like to add that convection, especially when combined with polymerization reactions, interfacial tension, and diffusion, can create a large variety of interesting phenomena that are investigated by different groups.[3−7]

A search of the literature related to chemical oscillations shows that we are not the first to be misguided by convection. Laplante and Pottier,[8] after many inconclusive experiments, introduced microdust particles into their cell and illuminated them with a laser to prove the existence of a convection cell. It was induced by the opening of the cell for inspection, resulting in evaporation of solvent that cooled the surface and caused a hydrodynamic instability. Further, Epstein et al.[9] found that the "photochemical oscillations" claimed by Bose et al.[10] and others were of the same physical origin. Convective movement of fluids should therefore be considered the rule rather than the exception: The common idea of the fluid at rest in a cuvette, moving only upon stirring, can be dangerously misleading.

Framework of Investigations. With investigations of azo compounds, we contribute to a major area of research, as documented by numerous publications and, e.g., the monograph on *Diazo Chemistry* by Zollinger.[11] The combination of the well-known organic azo chemistry with polymer science has led to a great variety of functional azo polymers.[12] One of the newer fields for azo polymers is the application for laser direct structuring or laser ablation.[13−15] Typical azo polymers for laser ablation are poly(arylazophosphate)s, poly(phosphorotriazene)s, poly(triazene)s, poly(azosulfide)s, poly(pentazadiene)s, etc. It has been suggested that, in addition to the photothermal properties, the photochemical properties (e.g., quantum yield of decomposition) are important for the sensitivity of these polymers.[16] Polymers containing chromophores that are sensitive to the laser radiation reveal the desired low ablation thresholds, allowing a better utilization of the laser photons.[17] The design of laser ablation polymers is mainly based on photochemical considerations and studies of model compounds. These model compounds are structurally closely related to the repetition units of the polymers. In previous investigations, the photochemical activity[18] and decomposition mechanisms[19] of various model compounds have been studied. The pentazadienes were identified as photochemically active compounds. The absorption band of the pentazadienes is in the range of common excimer laser wavelengths, i.e., XeCl (308 nm) and XeF (351 nm). Various pentazadiene model compounds and polymers have been investigated to elucidate the UV-induced decomposition pathway,[20] the thermolysis mechanism,[20] and the quantum yield of decomposition.[2]

Experimental Section

Materials. The pentazadiene and cinnamylidenemalonic ester polymer (CM polymer) have been synthesized according to procedures described elsewhere,[21,22] and their chemical structures are shown in Scheme 1. The polyester (PE polymer) was kindly provided by the BAYER AG and the hexachloroplatinum acid (H_2PtCl_6, HCPA) was purchased from Fluka.

Photolysis and Spectroscopy. Solutions of all compounds in THF (Merck spectroscopic grade) were irradiated in a commercial quartz cuvette (Starna GmbH), equipped with a temperature control. It has a volume of 2 mL, and the temperature control unit is located on the backside of the cuvette, with the front side facing the incoming laser beam. The path

* Corresponding author. Tel: 056-310 26 47. Fax: 056-310 44 16. E-mail: gassmann@psi.ch.

10.1021/jp013421r CCC: $22.00
Published on Web 03/29/2002

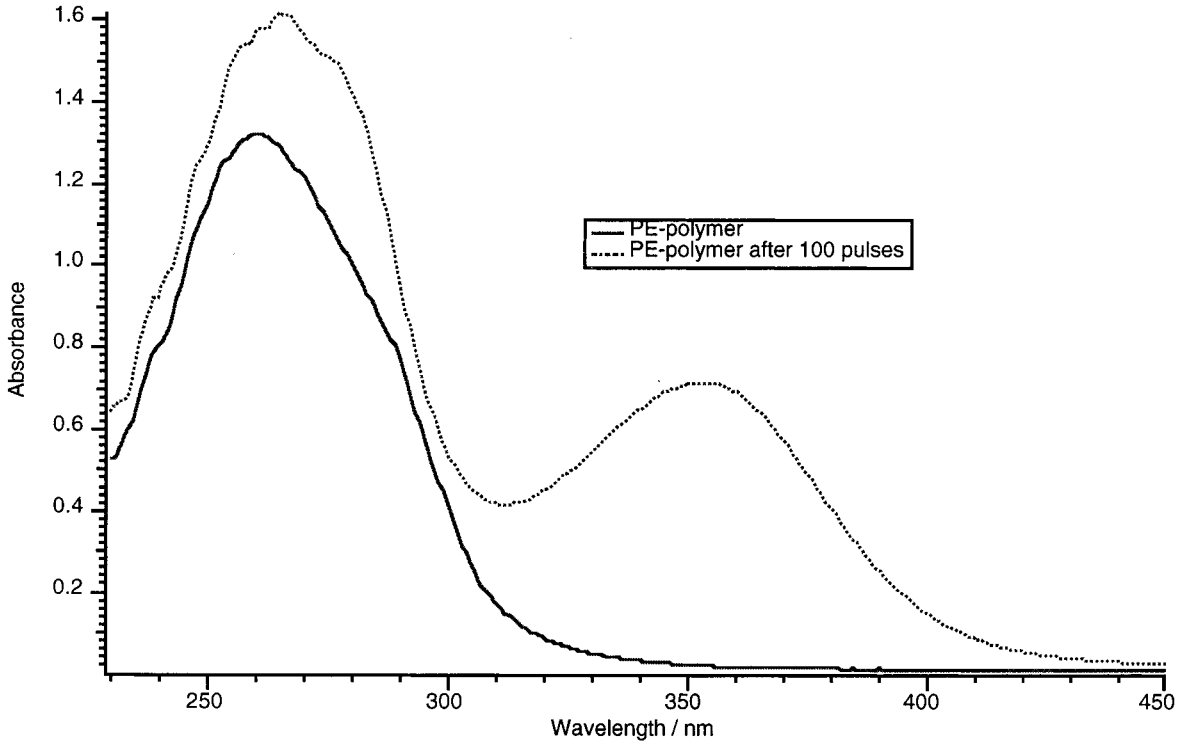

Figure 1. Photo-Fries rearrangement of the PE polymer. The growing peak at 350 nm (pointed line, after application of 100 pulses) is due to the new chemical structure shown in Scheme 2.

SCHEME 1: Chemical Structure of the Pentazadiene Compound (Top) and the CM polymer (Bottom)

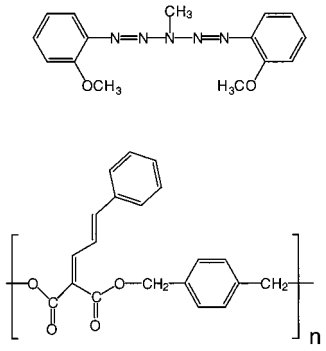

length for the detection is 10 mm (*y*-direction), while the path length for the laser beam is only 6.8 mm (*x*-direction). The concentrations were adjusted such that the UV−vis spectra could be recorded with an optical density of 1−1.5 (typically in the 10^{-5} M range). The UV irradiation source was a XeCl excimer laser (Lambda Physik, model Compex 205). The cuvettes were placed in a special aluminum sample holder (homemade), with fiber optic couplings perpendicular to the laser beam (at $x = 5$ mm, $z = 7.4$ mm). This detection path lies behind the vertical symmetry plane of the fluid ($x = 3.4$ mm). The UV−vis absorbance was recorded at selected wavelengths (i.e., at the absorption maxima of the compounds) with a diode-array spectrometer (Polytec, XDAP) with a sampling rate of 1 Hz over periods up to 1000 s. The detection wavelength was 384 nm for the pentazadiene, 325 nm for the CM polymer, and 280 nm for HCPA. For the PE polymer, the maximum of the growing band at 350 nm was used (cf. Figure 1). The cuvette was temperature-controlled by a thermostat (Lauda, model RML 6) in a temperature range from 15 to 55 °C.

Observations of Damped Absorption Oscillations. During many of our studies, unusual damped oscillations of the absorbance with periods of 30−60 s were observed after application of a laser pulse. They showed a clear temperature dependence and could only be observed within a temperature range from 8 to 45 °C. Further, they were detected in cuvettes with different thicknesses in the light propagation direction but disappeared upon stirring. Therefore, we evaluated various mechanisms responsible for these oscillations, i.e., chemical instabilities, gas evolution oscillators, and convection. Simulation of the oscillations using the first two mechanisms initially gave motivating results, but severe discrepancies with the experimental data remained. In our preliminary study[2] we classified convection as very unlikely, due to the extremely small temperature gradients induced by the incident laser light. However, after failure of all other explanations, we decided to reexamine the possibility of convection within the cuvettes, designed new experiments with additional compounds, and developed a model to simulate convection in small cuvettes.

Further Experiments To Test the Convection Interpretation. Many additional measurements, most of them based on the pentazadiene compound due to its large absorption oscillation amplitudes, were performed and compared with simulations. They were carried out at various temperatures, as a significant influence of temperature on the oscillation period was observed. Faster oscillations were detected at larger differences between the temperature of the thermostat and room temperature; no oscillations occurred when the temperature control was switched off or when the temperature control was adjusted exactly to room temperature. Repetition of the measurements after reduction of the amount of solution to ensure irradiation of the entire fluid (we used 0.8 mL instead of 1.9 mL) showed absorbance transients that quickly (within about 50 s) stabilized to the final level, exhibiting only small fluctuations or oscillations, resulting from homogenization of small absorption inhomogeneities due to decreasing laser intensities in *x*-direction (beam direction). Simulations reproduced the transients also for this situation. Further, mixing of

SCHEME 2: Scheme of the Photo-Fries Rearrangement of the PE polymer

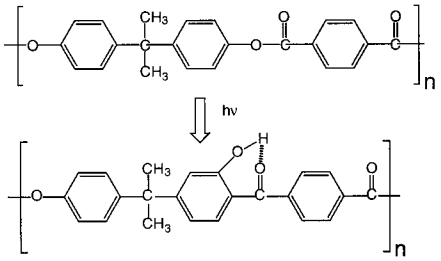

the fluid by stirring[2] also stopped ongoing oscillations, because of drastically accelerating the mixing process and so destroying the absorption inhomogeneities. All these observations gave clear indications for a convection-based mechanism.

In other experiments, we reduced the entrance window for the laser light to 20% of its normal area using 3 mm wide horizontal slits that were placed below or above the location of the spectrometer beam. To correct for the lost light, we applied 10−20 laser pulses (within 1 s) and observed oscillations at $T_S = 25$ and 37 °C with periods around 17 s for both slit locations. As these periods are clearly shorter than the simulated single-convection-cell period of 27 s (cf. Figure 4 below), they can be explained only by an additional physical mechanism leading to smaller and more intensive eddies. We assume an extra buoyancy (in addition to the heat deposition by absorption of laser energy already implemented into the simulation model, which is not negligible when multiple pulses are applied) attributed to N_2 bubbles[23] produced by photocleavage of pentazadiene. This extra buoyancy can disrupt the large convection cell and so result in complex spatiotemporal velocity fields containing smaller eddies leading to absorption variations with shorter wavelengths and therefore shorter observed oscillation periods, as could be confirmed by simulations (see below). To experimentally test the assisting role of gas bubbles for faster oscillations, a different compound was used. The PE polymer belongs to a class of compounds that undergo a Photo-Fries rearrangement upon UV irradiation[24] (shown in Scheme 2) and therefore produce no gaseous products. A growing UV absorption band at longer wavelengths, i.e., 350 nm (shown in Figure 1) can be assigned to this rearrangement. Experiments at higher temperatures with up to 100 pulses were performed, and oscillations with periods above 30 s were observed. This supports the above-mentioned hypothesis that oscillations with periods below the simulated values are caused by gaseous reaction products, which are absent in the case of a rearrangement reaction. In addition, gas bubbles could be seen in some experiments with the other compounds after heavy irradiation.

To rule out chemical oscillations unique to the pentazadienes or the PE polymers, various other photochemically active materials were tested. The inorganic compound HCPA as well as the polymer CM revealed damped oscillations similar to those observed for the pentazadiene compounds[2] (an example is shown in Figure 3 below, thicker line). The damped oscillations have lower amplitudes, probably due to the lower photochemical activity of these compounds. The fact that the oscillations can be observed for vastly different compounds added to our conviction that chemical oscillations must be excluded to explain the oscillations.

Model Section

Method for Simulation of Convection. For simulation of fluid convection, the Navier−Stokes equations together with transport equations for heat and matter have to be solved.[25] Equations and the method for their numerical integration are given in Appendix A. Due to symmetries in the experimental setup, simulation of fluid convection within the temperature stabilized quartz cuvette can be restricted to the two most important dimensions: the vertical (z) and the horizontal direction (x) parallel to the laser beam. In the x-direction, a temperature difference δT between the vertical back and front boundaries of the simulated fluid is driving a convection cell. Its physical origin is the temperature stabilization system consisting of a separate stabilization chamber at the back of the cuvette, through which water from a thermostat is pumped. It keeps the back wall of the experimental chamber at a controlled constant temperature T_S that can be set higher or lower than room temperature T_R, resulting in positive or negative δT, respectively. The front wall of the cuvette (where the laser beam enters), however, is not temperature stabilized and influenced by room temperature. To estimate δT, we equalize heat conduction within the fluid segment near the front wall (i.e., at $x = 0$) with heat flux between the front wall and the environment, which we approximate using the Stefan−Boltzmann law for blackbody radiation linearized around room temperature T_R

$$4\sigma T_R^{\,3}(T_S - \delta T - T_R) = K\left.\frac{\partial T}{\partial x}\right|_{x=0} \qquad \text{where}$$
$$\sigma = 5.67 \times 10^{-8}\ \mathrm{W\ m^{-2}\ K^{-4}} \quad (1)$$

The right-hand side of (1) can be evaluated during simulations, and the temperature of the front boundary of the fluid $T_S - \delta T$ is continuously adjusted using (1). An "effective" thermal conductivity K is used as a fitting parameter for adjusting simulations to our observations (see Table 1). To avoid instabilities during the initial simulation phase, simulations start with a nonmoving fluid with homogeneous temperature T_S. Within an initial time interval, a corrected temperature difference

TABLE 1: Physical Parameters

symbol	value	units	definition
η	0.46×10^{-3}	Pa s	dynamic viscosity of THF[a,b]
ν	5.2×10^{-7}	$m^2\ s^{-1}$	kinematic viscosity of THF[c]
γ	128×10^{-5}	K^{-1}	volumetric expansion coefficient of THF[a]
ρ	890	$kg\ m^{-3}$	density of THF[a]
K	0.6	$W\ m^{-1}\ K^{-1}$	"effective" thermal conductivity of THF[d]
c_H	1720	$J\ kg^{-1}\ K^{-1}$	heat capacity of THF[a]
D	15×10^{-9}	$m^2\ s^{-1}$	"effective" diffusion coefficient of pentazadiene in THF[e]
g	9.81	$m\ s^{-2}$	acceleration due to gravity
L	6.8×10^{-3}	m	width of experimental chamber (x-direction)
H	28×10^{-3}	m	height of THF column (z-direction)

[a] Beilstein Institut für Literatur der organischen Chemie, electronic data bank, 1998−1999. [b] The given value applies for 25 °C. For the simulations, η is considered as a quadratic function of temperature. [c] Calculated value using the relation $\nu = \eta/\rho$. [d] Molecular values for similar compounds found in the literature as, e.g., C_3H_8O and $C_4H_8O_2$ are about 25% of the given "effective" value for thermal conductivity. With the adopted value for K, the Prandtl number evaluates to $Pr = \nu/\kappa = 1.3$ (cf. eq 2 for the definition of κ). [e] The "effective" diffusion coefficient D describes the diffusion of pentazadiene in THF (D_{mol}) as well as the effect of microturbulence produced by the velocity gradients. The molecular value can be guessed to $D_{mol} \ll 10^{-9}\ m^2\ s^{-1}$ based on values found in the literature for compounds much smaller than pentazadiene. The effect of microturbulence must therefore be dominant and can be inferred approximately by comparison of measured and simulated damping of the oscillation (cf. Figure 3).

TABLE 2: Spectroscopic and Laser Parameters

symbol	value	units	definition
		Spectroscopic Parameters	
A_0	0.89		initial absorbance A (spectrometer readout value)[a]
$\hat{A}_{\lambda_{max}}$	0.17		absorbance at λ_{max} after destruction of all pentazadiene (needs ≈8 laser pulses[2])
$\hat{A}_{308}$	0.382		absorbance at 308 nm when all pentazadiene is destroyed (needs ≈8 laser pulses[2])
$\epsilon_{\lambda_{max}}$	29300	L mol^{-1} cm^{-1}	molar absorption coefficient[2]
α	0.317		fraction of destroyed pentazadiene[b] with one laser pulse[2]
β	0.21		factor for calculation of absorbance at 308 nm from absorbance at λ_{max}[c]
		Laser Parameters	
N	1−100		number of applied laser pulses
E	0.180	J	average energy of one laser pulse
δ_0	0.95		transmission of cuvette window

[a] $A = \epsilon cs$ where c = concentration of absorbing material [mol/L]; s = spectrometer path length, here $s = 1$ cm. [b] Concentration drop of pentazadiene due to one laser pulse is $\Delta c = -\alpha c$. [c] A linear relationship is assumed between variations of absorbance at $\lambda_{max} = 384$ nm and absorbance at 308 nm: $A_{308} = \hat{A}_{308} + \beta(A_{\lambda_{max}} - \hat{A}_{\lambda_{max}})$.

δT *f(t)* is applied, instead of δT from (1), with *f(t)* linearly increasing from 0 at $t = 0$ to 1 at $t = 5$ s. The following 145 s of simulation allows for stabilization of the convection cell; subsequently, the simulated laser pulse is applied. At this time point, the integration time step Δt is reduced by a factor of 5 for the following 40 s, and the laser energy is distributed over 100 (reduced) time steps to avoid numerical instabilities. To calculate the distribution of temperature increase and reduction of the absorption along the laser beam (x-direction), every single laser pulse fraction is further split into 10 parts, successively reducing the absorption and increasing the temperature. Parameters used for the simulations are given in Tables 1 and 2.

Simulations. A typical example for flow and temperature fields is given in Figure 2. Extensive investigations of the Rayleigh−Bénard convection,[26−28] (i.e., convection between two horizontal and parallel plates heated from below) show that the dimensionless Rayleigh number

$$Ra \equiv \frac{g\gamma\delta T H^3}{\nu\kappa} \quad \text{where} \quad \kappa \equiv \frac{K}{\rho c_H} \tag{2}$$

is the governing control parameter (definition of symbols cf. Table 1) for buoyancy-induced transport in a viscous fluid. In investigations of the Rayleigh−Bénard convection, δT is a **vertical** temperature difference between the bottom and the top boundary, and the aspect ratio *L/H* is normally **large**, whereas in our case, δT is a **horizontal** temperature difference, and the aspect ratio is **small** (between 0.1 and 1). For vertical temperature gradients, the basic physical state at small δT is pure heat conduction, and convective motion sets in at a critical Rayleigh number. However, in our situation with horizontal temperature gradients, a convection cell is created even by an arbitrarily small horizontal temperature gradient.[29] Theoretical reasons for this important difference for all aspect ratios *L/H* are given in Appendix B. It is further confirmed by other analytical calculations, numerical simulations, and comparisons with experiments.[30−32]

To help estimating convective velocities for situations with horizontal temperature gradients, we performed simulations with varied temperature differences δT (0.01−2 K), dynamic viscosities η (0.02×10^{-3} to 0.8×10^{-3} Pa s), densities ρ (300−2000 kg m^{-3}), volumetric expansion coefficients γ (10×10^{-5} to 200×10^{-5} K^{-1}), "effective" thermal conductivities K (0.05−1 W m^{-1} K^{-1}), heat capacities c_H (1000−3000 J kg^{-1} K^{-1}), widths of experimental chamber L (3−20 mm), and aspect ratios *L/H* (0.2−1). This sensitivity analysis led to the following relations for maximum (vertical) velocities v:

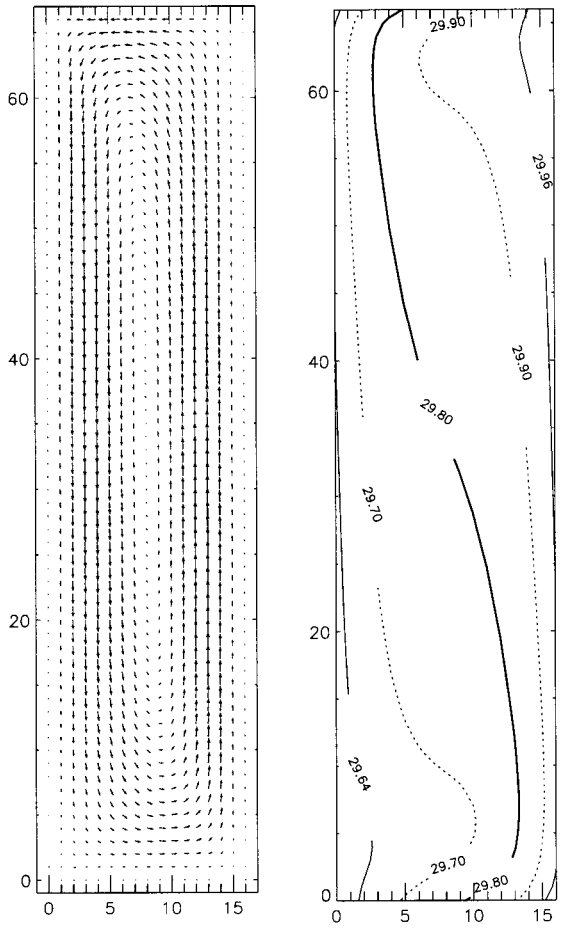

Figure 2. Cross section (x = horizontal versus z = vertical) of stationary velocity field (left) and temperature field (right) after stabilization of the convection cell. The temperature of the stabilization chamber (right side) is 30 °C, room temperature is 22.4 °C, giving 29.6 °C for the left wall based on eq 1. Coordinates are given as grid points 0−16 and 0−66 according to a 17 × 67 grid with a grid constant of 0.425 mm (i.e., the fluid within the cuvette has a cross section of 6.8 mm × 28 mm). The effect of boundary cohesion at the left, bottom and right walls results in vanishing velocities for grid points at $x = 0$, $x = 16$, and $z = 0$. Maximum velocities of 1.9 mm/s are found around $z = 33$, $x = 3$ and 13. The same value results from an estimate based on eqs 1 (giving $\delta T = 0.47$ K, when the gradient is approximated by $\delta T/L$) and 3 with parameter values from Table 1. The spectrometer beam is aligned parallel to y (i.e., perpendicular to the shown cross section) at coordinates $x = 12$, $z = 17$. The laser beam is parallel to x and enters from the left with almost homogeneous energy distribution between $z = 0$ and $z = 37$.

$$v \approx 5.3 \times 10^{-3} \frac{g\gamma\delta T L^2 \rho}{\eta} \quad \text{for} \quad Ra < 150\,000$$

$$v^2 \approx 2.7 \times 10^{-2} \frac{g\gamma\delta T H K}{\eta c_H} \quad \text{for} \quad Ra > 350\,000 \text{ and } \delta T \geq \text{ca. } 0.1 \text{ K} \tag{3}$$

The transition between small and large Rayleigh numbers occurs in the range 150 000−350 000. Instead of using *Ra* to select the appropriate formula, one can show that the relation giving the smaller velocities is correct for a large range of usual cuvettes. The flow field displayed in Figure 2 has been calculated for $Ra \approx 3 \times 10^6$; i.e., the relation for large *Ra*

applies. This relation was found also from other numerical simulations for vertical temperature gradients,[27] from analytical calculations for horizontal temperature gradients,[31] and from results from simple estimates based on the Bernoulli law. Our simulations with $Ra < 150\,000$ (small Ra) show negligible effects of K and c_H on v and linear relationships between v and ρ, γ, δT, and L^2. Here, L is the important geometrical parameter rather than H, because for very small δT (in the order of mK), viscous forces and buoyancy are in equilibrium in every horizontal cross-section of the fluid column. For the resulting low velocities (in the order of 0.1 mm/s), linearization of the dynamical equations is possible, making the relation plausible. The two coefficients in (3) have been calibrated with different numerical simulations and hold for v as the maximum velocity. The relations are useful to estimate convection velocities in small cuvettes induced by horizontal temperature differences.

The effective diffusion coefficient of pentazadiene in THF of $D \approx 15 \times 10^{-9}$ m^2 s^{-1} (cf. Table 1) results from a calibration to reproduce the experimentally observed damping of the absorbance oscillations by our simulations. Based on other numerical simulations,[33] the relation

$$\frac{D}{D_{\mathrm{mol}}} \approx \sqrt{Pe^*} \qquad \text{where} \qquad Pe^* = \frac{vH}{D_{\mathrm{mol}}} \tag{4}$$

holds over a large range of (modified) Péclet numbers and can be used to estimate the molecular diffusion coefficient D_{mol}:

$$D_{\mathrm{mol}} \approx \frac{D^2}{vH} \tag{5}$$

D_{mol} thus attains an order of magnitude of 10^{-11} m^2 s^{-1}, which is 3 orders of magnitude below D (cf. footnote e of Table 1).

Results

Damped Oscillations with Temperature-Dependent Periods. After irradiation of only the lower half of the solution (cf. Figure 2), the distribution of the absorption is inhomogeneous within the fluid after the laser pulse. The convection cell transports and mixes the two parts of the solution, resulting in damped absorbance oscillations at the spectrometer location. The resulting oscillation periods are directly coupled with the turnaround time of the convection cell, and the damping of the oscillation is due to diffusive mixing of the two parts of the fluid. The simulations show that a single laser pulse of 0.18 J has negligible effects on the temperature field (i.e., below 30 mK) and therefore has only a small influence on the stationary flow field produced primarily by horizontal temperature gradients caused by the temperature stabilization system. Figure 3 shows measured and simulated damped oscillations with a period of 37 s for the convection cell displayed in Figure 2. Due to different effects not taken into account in our simulations, differences between simulated and measured absorbances have to be expected. The simulated laser energy (the experimental laser produced pulses with an average of 0.18 J that varied ±10−20% between single pulses) was adjusted to reproduce the absorbance drop following the laser pulse, resulting in a reduced value of 0.13 J. The still remaining differences between observed and simulated absorbance oscillations are probably caused by uncertainties of the quantum yield (in the order of ±10%), and an unknown part of the radiation might be diffracted to the upper part of the cuvette that is not directly irradiated. Some photolysis might therefore occur also in the shaded part of the fluid and so lead to the observed lower first maximum. The roughly 10% higher level at which the absorption stabilizes might be due to photochemical trans−cis isomerization followed by a slow thermal relaxation. Both effects, supporting each other to reduce the amplitude of the absorbance oscillations, are not taken into account in our simulations. For improved estimates of the "effective" diffusion coefficient D, these effects would have to be quantified on the basis of additional measurements, demanding considerable changes in our experimental setup.

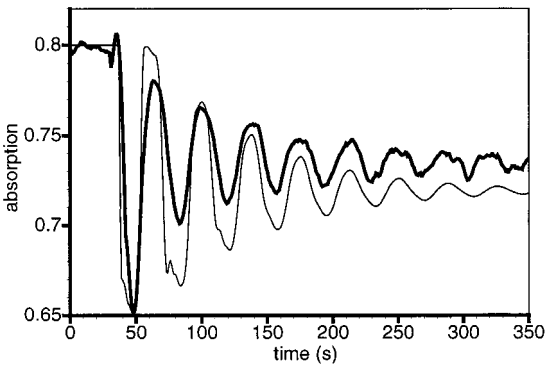

Figure 3. Measured (thicker line) and simulated damped oscillations of the absorbance with a period of 37 s after application of a laser pulse (at second 38) to a pentazadiene solution in THF stabilized to 27.7 °C. The simulated laser energy was adjusted to reproduce the absorbance drop following the laser pulse, and the simulated stabilization-chamber temperature was slightly increased to 30 °C to exactly reproduce the observed period (parameters cf. Tables 1 and 2). Using the maximum velocity of 1.9 mm/s (cf. Figure 2) and an estimate for the path length for one revolution of the fluid of 60 mm leads to a lower bound for the period of 32 s.

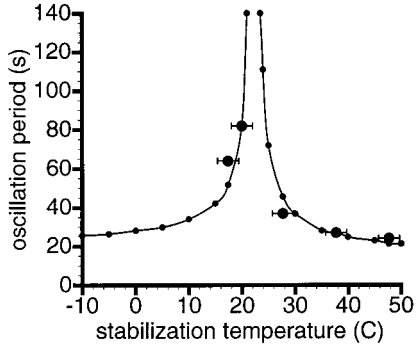

Figure 4. Measured (large points with error bars) and simulated (small points) periods of the absorbance oscillations for different temperatures of the stabilization chamber. If the thermostat pump is switched off, the stabilization temperature adjusts to room temperature ($T_R = 22.4$ °C) and no oscillations are present (equivalent to an infinitely long oscillation period). The calculated δT on the basis of eq 1 is nearly linearly related to the stabilization temperature T_S: $\delta T \approx a(T_S - T_R)$, with $a \approx 0.06$ between $T_R \pm 2$ °C, and $a \approx 0.04$ for T_S outside this interval.

Our simulations also reproduce the observed temperature dependence of the oscillation periods (Figure 4). We would like to point out that all simulations were made with a constant value for "effective" thermal conductivity K in our phenomenological heat exchange eq 1 and in the dynamical heat transport equation (cf. Appendix A). The adopted "effective" value for K (cf. Table 1) was calibrated for best matching the observed periods. The simulated points in Figure 4 are not symmetric around room temperature due to the decreasing viscosity of THF with increasing temperature. From the point of view of the application to photochemical laboratory praxis, the results clearly show that differences between thermostat and room temperatures have to be below 1 K to prevent convection disturbing the absorbance measurements. This implies that temperature differences δT between the back and front wall of the cuvette have to be below

60 mK (cf. caption of Figure 4). The error bars of ±2 K in Figure 4 result from estimates for the mismatch between δT calculated with eq 1 and the real but unknown δT. It also contains neglected effects related to the unknown temperature field within the sample holder as well as errors due to insufficient waiting time for establishing an exact thermal equilibrium.

Effects Due to Bubble Formation. To test our hypothesis that N_2 bubbles might reduce oscillation periods, we introduced bubble formation into our simulation model. The N_2 concentration is calculated from the absorbance difference, assuming that each cleaved pentazadiene molecule results in two N_2 molecules. These dissolved N_2 molecules are transported by the flow field and, immediately after creation, do not contribute to buoyancy, because no bubbles are formed yet. For nucleation theory, reference is made to Bowers et al.[23] To describe bubble formation and growth, we used a phenomenological bubble formation function

$$f_B(\tau) = \begin{cases} \tau^2 e^{-\tau} & \text{for } \tau < 1 \\ 1 - e^{-0.4587\tau} & \text{for } \tau > 1 \end{cases} \quad \text{with } \tau = \frac{t}{t_B} \qquad (6)$$

where t_B is a phenomenological bubble formation time and t means time after application of the laser pulse. The numerical constant 0.4587 ensures continuity of the function f_B at $\tau = 1$. For $f_B = 1$, the additional buoyancy is assumed to result from N_2 bubbles with atmospheric internal pressure; i.e., the bubbles are large enough such that surface tension can be neglected. However, we did not take into account any upward movement of the bubbles relative to the fluid. Both assumptions hold for bubble radii of a few micrometers. In this way, the above-mentioned short oscillation periods could be simulated using t_B on the order of 10−20 s, but a good fit to our observations could not be achieved with our two-dimensional simulations. It seems plausible that the third dimension has to be taken into account to correctly simulate small and intensive convection cells.

Conclusions

The results of different experimental series and the successful simulations of observed damped absorbance oscillations prove that the underlying mechanism is a purely physical convection cell induced by the temperature stabilizing system. Theoretical considerations show that any arbitrarily small horizontal temperature gradient induces convection. Simulations indicate that, in practice, convection can be neglected only if the temperature difference between the thermostat and room temperature is below 1 K (i.e., δT below 60 mK), which leads to oscillation periods longer than 2 min. In other words, a nonnegligible convection cell is always present when the thermostat is switched on and can give rise to large errors in photolysis experiments, when intensity differences of the incident light within the sample are present. In our case, where only 50% of the sample was irradiated, transport processes can result in errors of more than 20% in absorption spectra measured at one arbitrarily chosen time point after the laser pulse, leading, e.g., to errors in the quantum yield on the order of 50%. As our temperature stabilized cuvettes as well as our experimental procedure reflect standard procedures, our findings are a warning of a perhaps unexpected source of errors. Our analytical relations are useful to estimate periods of oscillations due to convective transport of concentration inhomogeneities in a large range of cuvette geometries and temperature differences and might help to prevent misinterpretation of photolysis experiments.

With an appropriate layout of the experimental setup, the convection cells investigated in this paper might be useful for indirectly estimating different properties that are difficult to measure in a straightforward way, as "effective" diffusion D, molecular diffusion D_{mol}, "effective" thermal conductivity K, and the volumetric expansion coefficient γ. For the latter, we found references differing up to 50%, and for the former three parameters, no indications were found in the literature.

Acknowledgment. This work has been supported by the Swiss National Science Foundation. We thank F. Geiger for the synthesis of the pentazadiene.

Appendix A

For our two-dimensional convection simulation model, we consider the Navier−Stokes equations under the Boussinesq approximation (A1) with velocities u and w for coordinates x and z, respectively, and transport equations (A2) for temperature T and concentration c (the concentration c of pentazadiene is linearly related to absorbance A):

$$\frac{\partial u}{\partial t} = -u\frac{\partial u}{\partial x} - w\frac{\partial u}{\partial z} - \frac{1}{\rho}\frac{\partial p}{\partial x} + \nu\Delta u$$

$$\frac{\partial w}{\partial t} = -u\frac{\partial w}{\partial x} - w\frac{\partial w}{\partial z} - \frac{1}{\rho}\frac{\partial p}{\partial z} + \nu\Delta w + g\gamma(T - T_0)$$

$$\frac{\partial u}{\partial x} + \frac{\partial w}{\partial z} = 0 \qquad \text{(A1)}$$

$$\frac{\partial T}{\partial t} = -u\frac{\partial T}{\partial x} - w\frac{\partial T}{\partial z} + \frac{K}{\rho c_H}\Delta T$$

$$\frac{\partial c}{\partial t} = -u\frac{\partial c}{\partial x} - w\frac{\partial c}{\partial z} + D\Delta c \qquad \text{(A2)}$$

Symbols and their numerical values are given in Table 1. The Laplace operator Δ refers in all our equations to the two dimensions x and z. Our method for solving the system (A1, A2) of partial differential equations is widely used in meteorology.[34] By introducing a stream function Ψ and a vorticity function ξ

$$u \equiv -\frac{\partial \Psi}{\partial z} \qquad w \equiv \frac{\partial \Psi}{\partial x} \qquad \xi \equiv \frac{\partial w}{\partial x} - \frac{\partial u}{\partial z} \qquad \text{(A3)}$$

into (A1), pressure p and the continuity equation can be eliminated and the integration of (A1) is reduced to integrating the dynamical equation for ξ

$$\frac{\partial \xi}{\partial t} = -u\frac{\partial \xi}{\partial x} - w\frac{\partial \xi}{\partial z} + \nu\Delta\xi + g\gamma\frac{\partial T}{\partial x} \qquad \text{(A4)}$$

and the Poisson equation

$$\xi = \Delta\Psi \qquad \text{(A5)}$$

(A5) is solved for a rectangular domain with quadratic grid cells using the IMSL-routine FPS2H.[35] For 17 × 67 grid points and 20 000 time steps (0.006−0.03 s), a simulation needs roughly 1 min CPU time on an Alpha 4100 computer. To take boundary cohesion into account, boundary conditions at the front, back, and bottom walls are coupled with respective velocities in such a way that even small velocities result in large corrections, forcing velocities to vanishingly small values.

Appendix B

The theoretical reason for the important difference between implied vertical and horizontal temperature differences is

explained in detail in Chandrasekhar,[25] where the following theorem is proved: *"Thermal instability as cellular convection will set in at the minimum (adverse) temperature gradient which is necessary to maintain a balance between the rate of dissipation of energy by all irreversible processes present and the rate of liberation of the thermodynamically available energy by the buoyancy force acting on the fluid."* We use this theorem to show that there is no critical horizontal temperature difference for a single convection cell to start (in contrast to Rayleigh−Bénard convection with vertical temperature differences, setting in only when a critical level is exceeded). For small temperature deviations from an average temperature T_0, the rate of liberation of thermodynamically available energy ϵ_L by the buoyancy force acting on the fluid is

$$\epsilon_L \propto \int_0^H \int_0^L w(x,z)(T(x,z) - T_0)\, \mathrm{d}x\, \mathrm{d}z \qquad \text{(B1)}$$

Because the temperature distribution for small velocities is approximately linear across the sample, the local temperature $T(x,z)$ can be approximated using the horizontal temperature difference δT between the back and front wall and the average temperature T_0

$$T(x,z) \approx T_0 + \left(x - \frac{L}{2}\right)\delta T \qquad \text{(B2)}$$

From (B1) and (B2) results

$$\epsilon_L \propto \delta T \int_0^H \int_0^{L/2} w(x,z)\left(x - \frac{L}{2}\right) \mathrm{d}x\, \mathrm{d}z \qquad \text{(B3)}$$

Due to symmetry reasons (i.e., velocity and temperature fields are symmetric to the plane $x = L/2$), the x-integration can be limited to $L/2$. Because w does not change sign within the restricted volume, $w(x,z)$ can be replaced by a typical medium velocity w_m and (B3) becomes

$$\epsilon_L \propto w_\mathrm{m} \delta T \qquad \text{(B4)}$$

According to eq 26 on p 196 in Chandrasekhar,[25] energy dissipation ϵ_D is proportional to the square of a similar typical medium velocity w_m

$$\epsilon_D \propto {w_\mathrm{m}}^2 \qquad \text{(B5)}$$

Following the above stated theorem, convection sets in at $\epsilon_D = \epsilon_L$. Using (B4) and (B5) this gives

$$w_\mathrm{m} \delta T \propto {w_\mathrm{m}}^2 \qquad \text{(B6)}$$

Even for very small temperature differences δT, there is always a convective solution with w_m different from zero

$$w_\mathrm{m} \propto \delta T \qquad \text{(B7)}$$

The proportionality constant depends on the properties of the fluid and the geometry only. In contrast, for vertical temperature gradients, analytical solutions lead to

$$\epsilon_L \propto {w_\mathrm{m}}^2 \delta T \qquad \text{(B8)}$$

and $\epsilon_D = \epsilon_L$ gives

$${w_\mathrm{m}}^2 \delta T \propto {w_\mathrm{m}}^2 \qquad \text{(B9)}$$

Different from (B6), (B9) has a solution with non vanishing w_m only, if δT meets a critical condition related to the well-known critical Rayleigh number. Though the above given reasoning is somewhat heuristic, it clarifies the point of much more involved exact analytical solutions.[25]

References and Notes

(1) Epstein, I. R. *Physica D* **1983**, *7*, 47.
(2) Kunz, T.; Hahn, C.; Baindl, A.; Nuyken, O.; Lippert, T.; Gassmann, F.; Wokaun, A. *J. Phys. Chem. A* **1999**, *103*, 4855.
(3) Martincigh, B. S.; Chinake, C. R.; Howes, T.; Simoyi, R. H. *Phys. Rev. E* **1997**, *55* (6), 7299.
(4) Komlósi, A.; Nagy, I. P.; Bazsa, G.; Pojman, J. A. *J. Phys. Chem. A* **1998**, *102*, 9136.
(5) Simoyi, R. H. *Pure Appl. Chem.* **1999**, *71* (6), 1007.
(6) Texier-Picard, R.; Pojman, J. A.; Volpert, V. A. *Chaos* **2000**, *10* (1), 224.
(7) Allali, K.; Volpert, V.; Pojman, J. A. *J. Eng. Math.* **2001**, *41*, 13.
(8) Laplante, J. P.; Pottier, R. H. *J. Phys. Chem.* **1982**, *86*, 4759.
(9) Epstein, I. R.; Morgan, M.; Steel, C.; Valdes-Aguilera, O. *J. Phys. Chem.* **1983**, *87*, 3955.
(10) Bose, R. J.; Ross, J.; Wrighton, M. S. *J. Am. Chem. Soc.* **1977**, *99*, 6119.
(11) Zollinger, H. *Diazo Chemistry*; Wiley-VCH: Weinheim, 1994.
(12) Kumar, G. S. *Azo Functional Polymers*; Technomic: Lancaster, PA, 1992.
(13) Nuyken, O.; Scherer, C.; Baindl, A.; Brenner, A. R.; Dahn, U.; Gärtner, R.; Kaieser-Röhrich, S.; Kollefrath, R.; Matusche, P.; Voit, B. *Prog. Polym. Sci.* **1997**, *22*, 93.
(14) Lippert, T.; Kunz, T.; Hahn, C.; Wokaun, A. *Recent Res. Dev. Macromol. Res.* **1997**, *2*, 121.
(15) Nuyken, O.; Dahn, U.; Hoogen, N.; Marquis, D.; Nobis, M. N.; Scherer, C.; Stebani, J.; Wokaun, A.; Hahn, C.; Kunz, T.; Lippert, T. *Polym. News* **1999**, *24*, 257.
(16) Lippert, T.; Stebani, J.; Ihlemann, J.; Nuyken, O.; Wokaun, A. *J. Phys. Chem.* **1993**, *97*, 12296.
(17) Wei, J.; Hoogen, N.; Nuyken, O.; Lippert, T.; Wokaun, A. *J. Phys. Chem. B* **2001**, *105*, 1267.
(18) Lippert, T.; Stebani, J.; Nuyken, O.; Stasko, A.; Wokaun, A. *J. Phototchem. Photobiol. A: Chem.* **1994**, *78*, 139.
(19) Stasko, A.; Adamcik, A.; Lippert, T.; Wokaun, A.; Dauth, J.; Nuyken, O. *Makromol. Chem.* **1993**, *194*, 3385.
(20) Baindl, A.; Lang, A.; Nuyken, O. *Macromol. Chem. Phys.* **1996**, *68*, 197.
(21) Baindl, A.; Lang, A.; Nuyken, O. *Macromol. Chem. Phys.* **1996**, *197*, 4155.
(22) Hoogen, N.; Nuyken, O. *J. Polym. Sci., Part A: Polym. Chem.* **2000**, *38*, 1903.
(23) Bowers, P. G.; Bar-Eli, K.; Noyes, R. M. *J. Chem. Soc., Faraday Trans.* **1996**, *92* (16), 2843.
(24) Rabek, J. F. *Mechanisms of Photophysical Processes and Photochemical Reactions in Polymers*; John Wiley & Sons: New York, 1987; p 594.
(25) Chandrasekhar, S. *Plasma Physics, Hydrodynamic and Hydromagnetic Stability, and Applications of the Tensor-Virial Theorem*; University of Chicago Press: Chicago, London, 1989; Vol. 4, pp 192−197.
(26) Velarde, M. G.; Normand, C. *Sci. Am.* **1980**, *243*, 78.
(27) Kerr, R. M. *J. Fluid Mech.* **1996**, *310*, 139.
(28) Henry, D.; Buffat, M. *J. Fluid Mech.* **1998**, *374*, 145.
(29) Mancho, A. M.; Herrero, H.; Burguete, J. *Phys. Rev. E* **1997**, *56* (3), 2916.
(30) Cormack, D. E.; Leal, L. G.; Imberger, J. *J. Fluid Mech.* **1974**, *65* (2), 209.
(31) Henkes, R. A. W. M.; Hoogendoorn, C. J. *Int. J. Heat Mass Transfer* **1993**, *36* (11), 2913.
(32) Braunsfurth, M. G.; Skeldon, A. C.; Juel, A.; Mullin, T.; Riley, D. S. *J. Fluid Mech.* **1997**, *342*, 295.
(33) Vannitsem, S.; Mareschal, M. *Phys. Rev. E* **1995**, *51* (6), 5564.
(34) Graber, W. K.; Portmann, W. *Meteorol. Zeitschr.* **1993**, *2*, 153.
(35) IMSL, *User's Manual, FORTRAN subroutines for mathematical applications*; IMSL Inc.: Houston, TX, 1991.